THE PENNSYLVANIA STATE UNIVERSITY
SCHREYER HONORS COLLEGE

DEPARTMENT OF AEROSPACE ENGINEERING

DETERMINATION OF MASS PROPERTIES FOR DOCKED SPACECRAFT WITH UNCOOPERATIVE OBJECTS

ROBERT VITAGLIANO
SPRING 2018

A thesis
submitted in partial fulfillment
of the requirements
for a baccalaureate degree
in Aerospace Engineering
with honors in Aerospace Engineering

Reviewed and approved* by the following:

David B. Spencer
Professor of Aerospace Engineering
Thesis Supervisor

Robert G. Melton
Professor of Aerospace Engineering
Honors Adviser

Amy R. Pritchett
Professor of Aerospace Engineering
Head of the Department of Aerospace Engineering

* Signatures are on file in the Schreyer Honors College.

ABSTRACT

Several conceptual space missions are proposing to dock with and capture an asteroid as part of a future asteroid mining mission. One of the main challenges of this process is how to control an asteroid of unknown properties once the spacecraft docks with it. Past work on the subject had determined the total mass and center of gravity of the combined system to within ten percent of their true values. In this work, the aforementioned mass properties are used to further define the mass properties of the system by determining the principal axes and principal moments of inertia. The spacecraft and asteroid are modeled using geometric shapes. A numeric simulation is then utilized to take into account the uncertainty in the total mass and center of mass location by running several iterations of the calculation based on a normal distribution centered around the true values. The results are then compared to the true principal moments of inertia and principal axes.

TABLE OF CONTENTS

LIST OF FIGURES

LIST OF TABLES

ACKNOWLEDGEMENTS

Completing a piece of research always requires assistance and encouragement from many people, so I'd like to take this opportunity to thank:

Dr. David Spencer, my thesis supervisor, for offering his advice, guidance, and time, to ensure that I was always moving forward and doing quality work. Your help has been invaluable and I could not have completed this thesis without you.

Dr. Robert Melton, my honors advisor and faculty reader, for his academic guidance throughout my time at Penn State and for inspiring my interest in astrodynamics during my junior year.

Dr. Joseph Ranalli, for giving me my first research experience as a sophomore at Penn State Hazleton. Working with you gave me the skills and confidence to take on another research project and know that I would be succeed.

My parents and my brother, Nicolas, for always offering their love and support throughout everything I've done in my life. Nick, in three years, I hope to see your thesis next to mine.

My girlfriend, Cassidy, who has supported me throughout all the challenges of my research and has always believed in me.

My roommate, Mauro, who made sure that I actually slept once in a while and survived senior year. I hope someday I reach your age and your height.

Chapter 1

Introduction

As modern society continues to grow and advance technologically, so too does its need for natural resources, specifically precious metals and other minerals. Gold, silver, and copper are all key components in the production of electronics, being used in connections on microprocessors, wiring, and thermal control systems. Aluminum has been used in aircraft constuction since the all-aluminum engine block used on the Wright Flyer in 1903. Due to its high strength to weight ratio, we have also recently seen an increase in demand for aluminum from the automobile industry as manufacturers move away from steel in efforts to create lighter, more fuel-efficient vehicles.

For all of history, the earth's deposits of these materials have been the only source available and the only source needed to meet human usage. As spacecraft travel further and further on their missions, it becomes both mission limiting and incredibly expensive to launch everything needed to complete a mission from Earth. A space-based source for resources such as water and building materials would allow for structures to be built that could serve as a refueling station for chemical propulsion spacecraft or a replenishment stop on manned missions. One of the most popular solutions being explored is asteroid and planet mining. Luxembourg recently invested millions of Euros into a private company focused on asteroid mining and aims to launch a prospecting mission by the year 2020 [1]. Currently, NASA's OSIRIS-Rex mission is scheduled to dock with a Near Earth Asteroid (NEA), Bennu, in the fall of 2018 to retrieve regolith samples that will be transported back to Earth for composition analysis [2]. While this mission's objectives are purely

scientific, the same type of mission could be structured to search for large concentrations of usable resources.

A major issue regarding the cost effectiveness of a mining operation is the cost of sending equipment to and returning the mined material to a more useful location in space (i.e. Cis-Lunar space vs. the asteroid belt). There is also a higher chance of system failure, the need for a more complex system, and the potential loss of a spacecraft the further from Earth it needs to travel. To remedy these obstacles, it could be beneficial if an asteroid could be moved into a stable orbit around the Earth, Moon, or even Mars [3]. However, this introduces an interesting challenge: docking with, controlling, and moving an asteroid without knowing its exact composition, mass, or mass distribution.

Past work on the subject by Wittick [4] developed a technique that utilized a combination of short, impulsive thrusts and accelerometers onboard the docked spacecraft to determine the total mass of the spacecraft-asteroid system and also the center of mass of the combined system. This technique was tested in simulation and was capable of determining the aforementioned properties to within 10% of their true values. This thesis focuses on analyzing the determination of additional mass properties of the asteroid-spacecraft system assuming a spacecraft of known mass properties has already successfully docked with the uncooperative asteroid. Specifically, it demonstrates how to determine the new principal axes and moments of inertia (MOIs) and investigate how the errors previously seen in calculating the new center-of-mass affect the previous two properties.

To analyze the most general case and simulate the most realistic docking scenario, the principal axis systems of the spacecraft and asteroid are assumed to be misaligned with one another, expressed as an arbitrary 3-1-3 Euler rotation. Both the spacecraft and asteroid are assumed to be rigid bodies to eliminate any effects of deformation with an inextensible, vibration

free coupling system connecting them, allowing the combined system to truly behave as a single body. A randomized, normal distribution of center-of-mass locations and system masses is generated to simulate an error in these values on the same order of uncertainty that can result from Wittick's linear deterministic model. Error in center-of-mass location and error in system mass are looked at independently first and then considered simultaneously. For all these cases, the combined system center-of-mass location and the mass of the system will be utilized in order to solve the eigenvalues and eigenvector problem to determine the principal axes and principal moments of inertia (MOIs) of the system. Finally, the results from each of the error cases are compared against the true values of these quantities and the differences are quantified and visualized to look at how the initial uncertainty in mass properties propagates through the calculations.

Chapter 2

Background

Several studies have investigated portions of this problem or similar ones in the past. Work by Liang and Ma [5] investigated the dynamics of an autonomous docking repair satellite rendezvousing with another uncooperative and tumbling satellite. The focus of that research was to develop an adaptive control method that could be used to track and determine the angular velocity of the tumbling satellite. This tracking is necessary so the repair satellite can make its own angular velocity adjustments to eliminate the relative angular velocity between the two bodies and facilitate a smooth docking procedure.

The Database of Asteroid Models from Inversion Techniques (DAMIT) similarly attempted to create a database for the astronomical community that included accurate physical models of asteroids [6]. For the majority of the asteroids, all information about them comes from time-resolved photometry, using a lightcurve inversion method to determine the physical attributes such as size, spin state, and spectral state. While useful for planning a spacecraft rendezvous maneuver, this data still lacks any information about density, mass, or other mass properties necessary to fully characterize an asteroid in order to control it with a docked spacecraft.

Even solely looking at shape and size data, DAMIT is a growing database and it currently has a limited catalog of objects. This limitation makes it necessary to have other methods of determining asteroid shapes and sizes, as this information is critical to making an initial guess of the inertia tensor. One option is to utilize a series of high resolution images from the Hubble Space Telescope similar to the method used to gather information on Vesta in 1994 [7]. 56 images were

taken over the course of 71 hrs. and used to find the radii of the elliptical asteroid to within ±12 km of uncertainty. While this level of detail may not be usable for smaller bodies, a high-resolution camera system implemented on a spacecraft could perform a more refined shape assessment on approach to the asteroid. That data can then be used by either the computer on the spacecraft or mission control to make an initial guess of the inertia tensor of the asteroid.

A well-documented scenario involving control of uncooperative objects occurred during the Apollo 13 mission in April 1970. Nearly 56 hours after launch, an oxygen tank on the Command and Service Module (CSM) exploded, causing a failure of another oxygen tank, which proceeded to rapidly leak into space [8]. The declining oxygen levels forced the crew to shut down the CSM and move into the Lunar Module (LM) where they were able to use the resources that were planned for their stay on the moon's surface.

The original flight plan for Apollo 13 included a free return trajectory, however the oxygen tank failure occurred after a midcourse correction had been made to move the spacecraft into its lunar landing course. Aside from the limited quantities of power, water, and oxygen, the crew also had to use the control system of the LM to guide the combined CSM and LM system back to Earth. The key difference between Apollo 13 and the challenge proposed in this thesis is that the mass properties of both bodies (the CSM and LM) were known with relative accuracy. Some uncertainty existed as to how mass of the tank was lost in debris due to the explosion but generally masses, mass distributions, centers-of-mass, and moments of inertia had all been calculated and were available to the engineers in the ground as they worked to develop a new control scheme. In later sections, this example will be modeled using simple geometric volumes in SolidWorks and the principal MOIs of the CSM and LM will be calculated using the built-in software tools. Then these

same models will be inputted into the simulation software developed to calculate the same values and test the simulation results.

Chapter 3

Model Analysis

This chapter begins by defining the mathematical models for the asteroid, spacecraft, their respective coordinate systems, and the same quantities for the combined system as well. Next the known properties of the models will be stated, along with any assumptions made and the uncertainty in these values. Finally, the process of determining the principal axes and principal MOIs will be discussed.

Asteroid and Spacecraft Models

Within the scope of this study, two separate asteroid mass models are considered: a dumbbell shaped mass model (Fig. 1) and a purely spherical model (Fig. 2). Let the $\hat{a}_n$ vectors define the principal axis system of the asteroid for both models, with the origin of the axis system located at the center of mass.

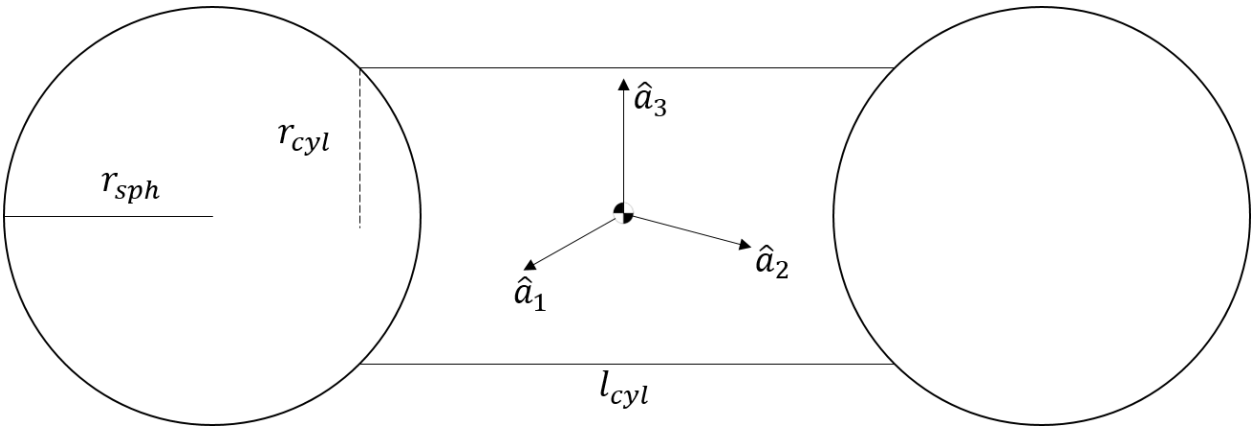

Figure 1: Dumbbell Asteroid Model

Both models also assume a constant density throughout the structure of the asteroid; while this limits the direct applications of this research, variable density could be accounted for in the future by modifying the inertia matrices.

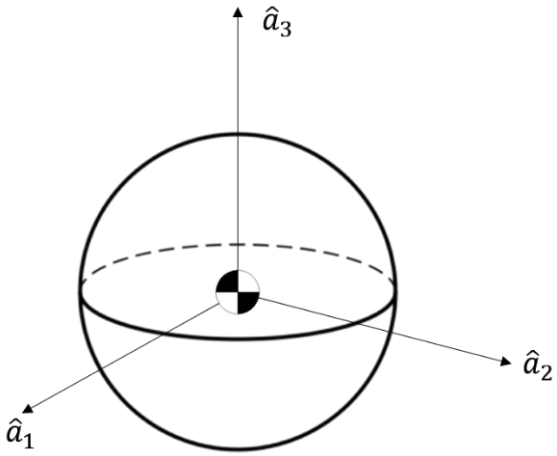

Figure 2: Spherical Asteroid Model

The inertia tensor for the dumbbell model is defined as:

$$I_a = M_a \begin{bmatrix} \frac{4}{15}r_{sph}^2 + \frac{l_{cyl}^2}{36} + \frac{2}{3}\left(r_{sph} + \frac{l_{cyl}}{2}\right)^2 & 0 & 0 \\ 0 & \frac{4}{15}r_{sph}^2 + \frac{l_{cyl}^2}{36} + \frac{2}{3}\left(r_{sph} + \frac{l_{cyl}}{2}\right)^2 & 0 \\ 0 & 0 & \frac{r_{cyl}^2}{6} + \frac{4}{15}r_{sph}^2 \end{bmatrix} \quad (1)$$

which is a function of several physical properties of the asteroid, including the mass of the asteroid (M_a), the radius of the spherical ends of the dumbbell (r_{sph}), the length of the cylindrical rod connecting the spheres (l_{cyl}), and the radius of the rod (r_{cyl}). The spherical mass distribution seen in Eq. (2) is symmetric about all three axes and is only dependent on the mass of the asteroid (M_a) and the radius of the sphere (r_{sph}).

$$I_a = \begin{bmatrix} \frac{2}{5} M_a {r_{sph}}^2 & 0 & 0 \\ 0 & \frac{2}{5} M_a {r_{sph}}^2 & 0 \\ 0 & 0 & \frac{2}{5} M_a {r_{sph}}^2 \end{bmatrix} \quad (2)$$

For ease of notation, either asteroid inertia matrix can be substituted with the general form:

$$I_a = \begin{bmatrix} I_{a_1} & 0 & 0 \\ 0 & I_{a_2} & 0 \\ 0 & 0 & I_{a_3} \end{bmatrix} \quad (3)$$

For the spacecraft that will dock with the asteroid, it will be modeled as a cylinder of uniform density (Fig. 3). The uniform density simulates the balance of components about the center of mass that is generally seen in spacecraft of this shape. Let the $\hat{b}_n$ vectors define the principal axis system of the spacecraft, with the origin of the axis system located at the center of mass seen in Figure 3.

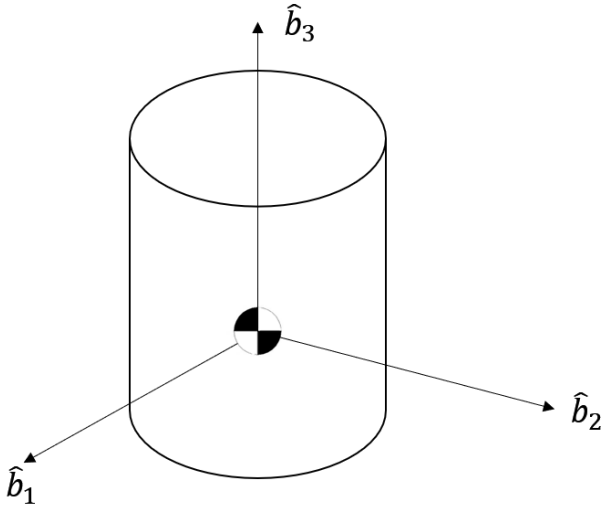

Figure 3: Cylindrical Spacecraft Model

The inertia tensor in Eq. (4) is a function of the spacecraft mass (M_s), the length of the cylinder (l), and the radius (r).

$$I_s = \begin{bmatrix} I_{s_1} & 0 & 0 \\ 0 & I_{s_2} & 0 \\ 0 & 0 & I_{s_3} \end{bmatrix} = M_s \begin{bmatrix} \frac{(3r^2 + l^2)}{12} & 0 & 0 \\ 0 & \frac{(3r^2 + l^2)}{12} & 0 \\ 0 & 0 & \frac{r^2}{2} \end{bmatrix} \quad (4)$$

Known Properties

In order to determine the principal axes and MOIs of the combined system, first it is assumed that the spacecraft mass (M_s) is known. The combined system mass (M_{total}), and location of the system center-of-mass, expressed as a vector ($\boldsymbol{r_{cm}}$) from the spacecraft center-of-mass in the $\hat{b}_n$ frame, have been determined using Wittick's methodology. M_a is simply determined by finding the difference between the total mass of the system and the mass of the spacecraft:

$$M_a = M_{total} - M_s \quad (5)$$

Next, a vector $\boldsymbol{r_a}$ is defined as beginning at the center of mass of the spacecraft and extending to the center of mass of the asteroid. Due to the rigid body assumption, the vector from the spaceraft center of mass to the location of the combined system center of mass must be a constant multiple of vector $\boldsymbol{r_a}$. It is possible to express this relation as:

$$\boldsymbol{r}_{cm} = \frac{M_a}{M_a + M_s}\left(r_{a_1}\hat{b}_1 + r_{a_2}\hat{b}_2 + r_{a_3}\hat{b}_3\right) \quad (6)$$

and then algebraically find $\boldsymbol{r_a}$, a necessary component in defining the inertia matrix of the total system later on in this model.

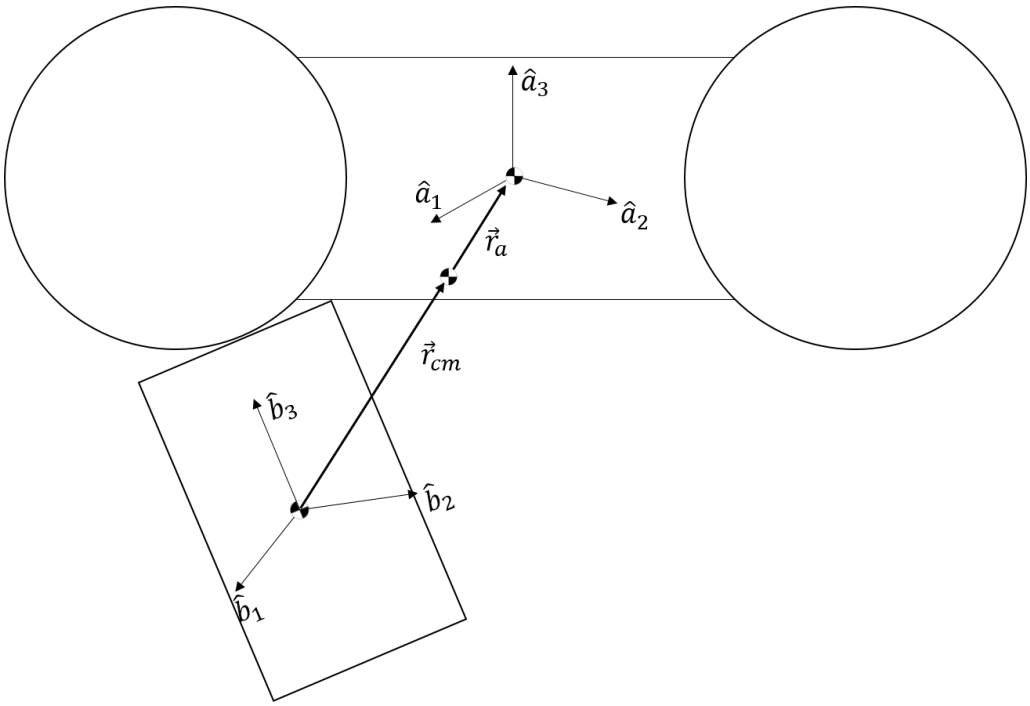

Figure 4: Spacecraft Docked with Dumbbell Asteroid

Combined Body and Orientation

The spacecraft is assumed to have docked with the asteroid in an unknown orientation relative to the asteroid's principal axis system. The orientation of the spacecraft ($\hat{b}$ frame) can be expressed as a 3-1-3 Euler rotation using the angles $\psi,\ \theta,$ and ϕ with respect to the asteroid ($\hat{a}$ frame). The $\hat{t}$ frame serves as an intermediate coordinate system.

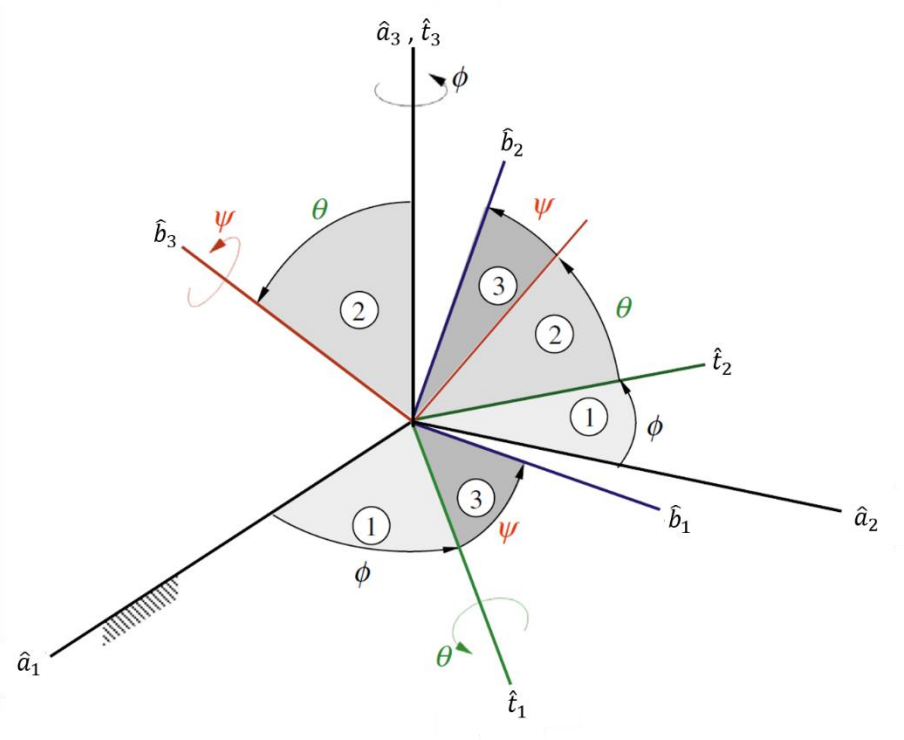

Figure 5: Euler 3-1-3 Rotation [9]

Therefore, the direction cosine matrix $C_{b/a}$ is expressed in terms of these rotation angles in Eq. (7) to transform the asteroid's reference frame into that of the spacecraft, where c( ) represents cosine of the angle and s( ) is sine of the angle.

$$C_{b/a} = \begin{bmatrix} c\phi\, c\psi - \mathrm{s}\phi\, \mathrm{c}\theta\, s\psi & \mathrm{s}\phi\, \mathrm{c}\psi + \mathrm{c}\phi\, \mathrm{c}\theta\, s\,\psi & \mathrm{s}\,\theta\, \mathrm{s}\,\psi \\ -\,\mathrm{c}\,\phi\, s\psi - \mathrm{s}\,\phi\, \mathrm{c}\,\theta\, \mathrm{c}\,\psi & -\,\mathrm{s}\,\phi\, \mathrm{s}\,\psi + \mathrm{c}\,\phi\, \mathrm{c}\,\theta\, \mathrm{c}\,\psi & \mathrm{s}\,\theta\, \mathrm{c}\,\psi \\ \mathrm{s}\,\phi\, \mathrm{s}\,\theta & -\,\mathrm{c}\,\phi\, \mathrm{s}\,\theta & \mathrm{c}\,\theta \end{bmatrix} \tag{7}$$

Then the matrix multiplication seen in Eq. (8) is performed to rotate I_a such that it will then align with the $\hat{b}$ frame.

$$I_a^b = C_{b/a} I_a C_{b/a}^T \tag{8}$$

However, the inertia tensors are still expressed about two separate axis systems, so the parallel axis theorem is applied to determine the total inertia matrix ($\boldsymbol{I}_{cm}$) about the combined body's center of mass. To simplify this expression, the constant μ is defined as:

$$\mu = 1 - \frac{M_a}{M_a + M_s} \tag{9}$$

allowing $\boldsymbol{I}_{cm}$ to be calculated and expressed element by element:

$$I_{cm_{jk}} = I_{s_{jk}} + I^b_{a_{jk}} + r_{a_j} r_{a_k} [M_s(1-\mu)^2 + M_a \mu^2] \tag{10}$$

The j and k subscripts in Eq. (10) are integers from 1-3, representing the index of the rows and columns of the total inertia tensor, respectively.

Mass Property Determination Process

Now that the total inertia tensor of the system has been defined in a single reference frame, the principal MOIs and principal axes can now be determined by solving for the eigenvalues (λ_i) and eigenvectors ($\hat{p}_i$) of $\boldsymbol{I}_{cm}$. To find the principal MOIs, the following relation must be satisfied:

$$det \begin{bmatrix} \lambda_1 - I_{cm_{11}} & I_{cm_{12}} & I_{cm_{13}} \\ I_{cm_{21}} & \lambda_2 - I_{cm_{22}} & I_{cm_{23}} \\ I_{cm_{31}} & I_{cm_{32}} & \lambda_3 - I_{cm_{33}} \end{bmatrix} = 0 \tag{11}$$

$$\begin{bmatrix} \lambda_1 - I_{cm_{11}} & I_{cm_{12}} & I_{cm_{13}} \\ I_{cm_{21}} & \lambda_2 - I_{cm_{22}} & I_{cm_{23}} \\ I_{cm_{31}} & I_{cm_{32}} & \lambda_3 - I_{cm_{33}} \end{bmatrix} \begin{bmatrix} \hat{p}_1 \\ \hat{p}_2 \\ \hat{p}_3 \end{bmatrix} = \begin{bmatrix} 0 \\ 0 \\ 0 \end{bmatrix} \tag{12}$$

while Eq. (12) is used to determine the principal axes. MATLAB or other similar software can be implemented to numerically calculate these mass properties for the combined system.

Chapter 4

Simulation Setup

Now that the models and methods for determining the mass properties of the system have been defined, the actual algorithm used in the MATLAB simulation can be presented. First, the known properties of the system (total system mass and center-of-mass location) are inputted into the function. Next, the program enters into a loop that will run for as many cases as the user wishes to use in the Monte Carlo simulation, which will be discussed in depth in the following sub-section. Inside the loop, either the center-of-mass location vector, total system mass, or both are varied according to their known uncertainties. Then the inertia tensors for both the spacecraft and asteroid are calculated individually based on their geometric properties and masses.

The three Euler angles are then defined based on the orientation of the spacecraft when it docked with the asteroid and they are used to generate the DMC to transform the asteroid reference frame (a) into the spacecraft reference frame (b). The parallel axis theorem is applied to account for the combined system center-of-mass's distance from the origin of the spacecraft's reference frame. Finally, MATLAB's built in eigenvalue and eigenvector solver is employed to determine the principle MOIs and axes from the combined system inertia matrix and those mass properties are stored for that run. This ends the functionality within the loop, which will then run again if it still needs to generate more cases or move on if the predetermined number of cases have been run.

Once outside of the loop, the errors in the mass properties for each case are calculated by comparing the results from each run with the varied inputs to the results of the run made with the "true" or "correct" inputs. From there the results are plotted and visualized into a collection of graphs and figures. The overall flow of the simulation is presented in Figure 6.

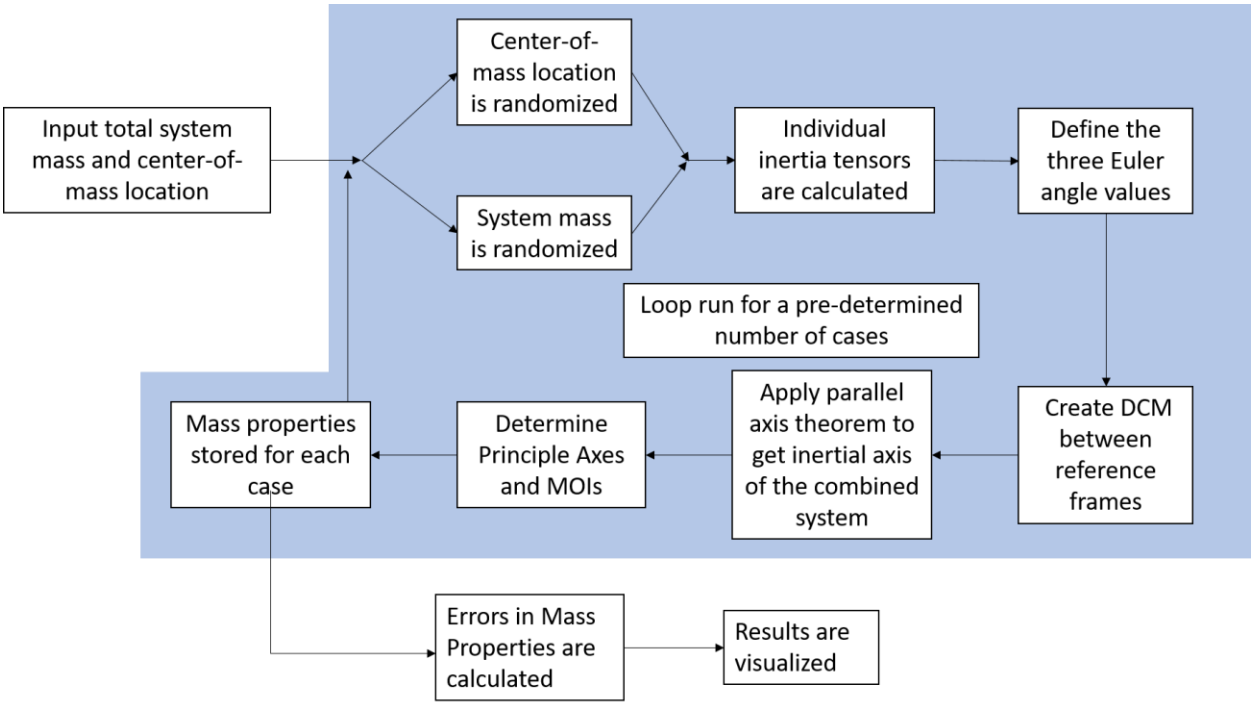

Figure 6: Simulation Flow Chart

Monte Carlo Method

As previously mentioned, the combined system mass and center-of-mass location of the combined system is only known to within 10% of their true values. To analyze the effect of this uncertainty on the calculations performed in this simulation and the possible errors it may cause in the principle MOIs and axes, a Monte Carlo simulation was utilized to create 50 cases simulating the uncertainty of the known quantities. Variations in system mass and center-of-mass location can be considered individually to see the effects of each variable or simultaneously to simulate the most realistic scenario.

When taking into account the uncertainty in the center-of-mass location, a random number generator is used to generate a number, with zero mean, serving as the uncertainty factor. This uncertainty factor is then scaled by 10% of the individual vector component of $\boldsymbol{r_{cm}}$ that it is

randomizing. Uncertainty factors are generated and scaled for all three components of $\boldsymbol{r_{cm}}$. Finally, each of these three components are combined together into a randomizing vector, which is then added to the correct $\boldsymbol{r_{cm}}$ to create the new $\boldsymbol{r_{cm}}$ for that case.

The mass randomization follows a similar process: the same random number generator creates an uncertainty factor, that factor is scaled by 10% of the total system mass, and then added to the asteroid mass. This factor is only added to the asteroid mass and not the total system mass because it is assumed that the mass of the spacecraft is well defined, meaning the uncertainty must solely affect the asteroid mass estimate.

Chapter 5

Apollo Testing

To validate this software simulation, the Apollo 13 CM and LM were modeled using simple geometric shapes in SolidWorks based on the actual shapes, sizes, and masses of these components prior to the CM/LM undocking before re-entry. The principle MOIs and principle axes were then determined using the built-in mass property evaluation tool and compared to the results obtained from the MATLAB simulation.

LM and CM Models

The actual CM was conical in shape, with the docking port that was connected to the LM located where the tip of the cone would have been. In this scenario was modeled as a solid cone of uniform density with a height of 3.65m, a radius of 1.95m, and a mass of 5610kg. The LM was actually comprised of three separate sections: the descent stage, midsection, and the ascent stage. Each section had varying geometries with additional extrusions like the landing legs, communication antenna, and support structure. However considering that is was relatively axisymmetric and was able to collapse to fit inside the payload fairing during launch, was modeled as a solid cylinder of uniform density with a height of 4.5m, a radius of 2.1m, and a mass of 11179kg. Modeling both with more complex geometries and more realistic mass distributions (i.e. accounting for fuel tanks, material densities, astronaut location within the spacecraft, etc.) would yield more accurate results. However, considering that the larger goal is to generate an initial guess

of the mass properties of an asteroid utilizing geometric models, that same approach was taken here to gauge the simulation's capability.

Simulation Results

Both the MATLAB simulation and SolidWorks models calculated the principle moments of inertia to within approximately 6% or less of the values given in the Apollo 13 Flight Report [8]. More significantly, the MATLAB Simulation and SolidWorks models were nearly identical, with only a difference of 2 $kg \cdot m^2$ in both the $\boldsymbol{I_{yy}}$ and $\boldsymbol{I_{zz}}$. This demonstrates that the deviations from the flight data come from the assumptions made by using geometric approximations for the LM and CM, as the two geometric models agree.

Table 1: Apollo 13 Principle MOIs

MOIs ($kg \cdot m^2$)	**MATLAB Simulation**	**Flight Report Values**	**SolidWorks**
$\boldsymbol{I_{xx}}$	31050	32439	31050
$\boldsymbol{I_{yy}}$	134783	127437	134785
$\boldsymbol{I_{zz}}$	134783	129499	134785

Table 2: Principle MOIs Errors

	MATLAB Simulation	**SolidWorks**
$\boldsymbol{I_{xx}}$	4.28%	4.28%
$\boldsymbol{I_{yy}}$	5.76%	5.77%
$\boldsymbol{I_{zz}}$	4.08%	4.08%

Chapter 6

Results

Dumbbell Model

As the accuracy of the known mass properties used as the basis of this method come from the results of Wittick's work [4], one of the same asteroid and spacecraft models from that study are utilized here to ensure that the same accuracy assumptions are applicable. The spacecraft model has a height of 5.9m, radius of 1.35m, and a mass of 15000kg. The dumbbell asteroid model has a mass of 10000kg, the end sphere radius of 1m, and the connecting central cylinder has a radius of 0.5m and a length of 1m. Both the center-of-mass vector and total system mass are held constant at their true values in each run unless specifically stated that one is being varied.

Varying Center-of-Mass Location

In this series of 50 cases run through the simulation, the center-of-mass (COM) location was varied via the Monte Carlo process described earlier. The variations between the system COM locations are seen in Fig. 7, as well as the approximate locations for the spacecraft and asteroid COMs. Each line is a visualization of the $\boldsymbol{r_a}$ vector for an individual case, plotted in 3D space, physically showing the amount of uncertainty that exists in the COM location for the spacecraft, total system, and asteroid. Although the initial mass properties were shown to be known with an

uncertainty of 10%, values beyond this were included in these results to give additional insight to the behavior of the desired quantities if larger uncertainty is introduced into the system.

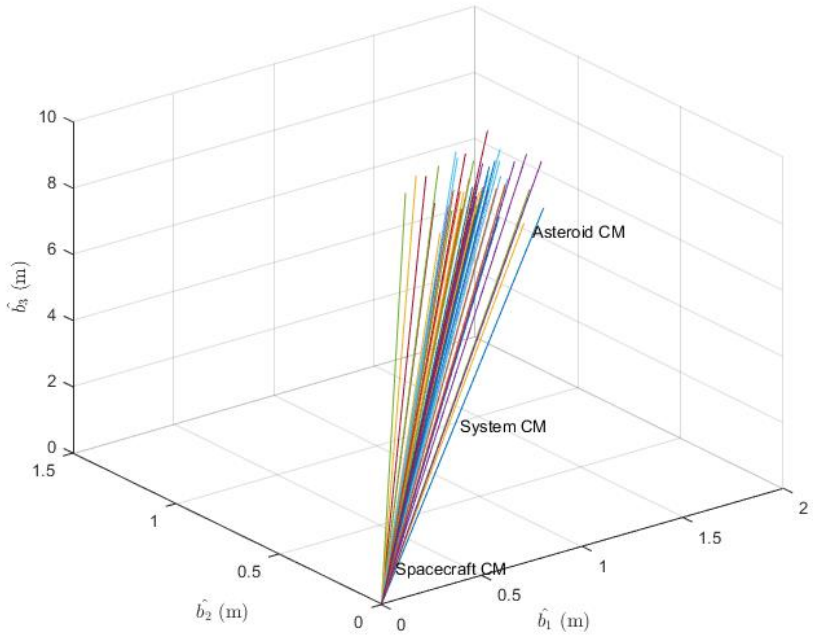

Figure 7: Center-of-Mass Vectors

Figure 8 demonstrates the correlation or lack thereof between the percent magnitude error in the COM location and each of the principal MOIs. After the simulation calculated the three principal MOIs for each case, the absolute difference between the associated MOI and the true value was determined. This difference was then normalized with respect to the true value and converted to a percentage to allow the results to be more easily contextualized. These percent errors are then plotted as a function of the percent difference in magnitude of the $\boldsymbol{r_{cm}}$ vector for each case and the true $\boldsymbol{r_{cm}}$. The difference in magnitude of $\boldsymbol{r_{cm}}$ was chosen as the independent variable in these plots, as opposed to individual vector component differences in the COMs, because more than one component is utilized when applying the parallel axis theorem. This

coupled behavior means the principal MOIs can be affected by errors along two of the three axes simultaneously, which can be accounted for by comparing the vector magnitudes.

Both I_{yy} and I_{zz} have a near linear relationship between the input and output errors, reaching approximately 15% MOI error with 10% error in the COM location. I_{xx} , conversely, seems to be affected very little by varying the COM, as there is no noticeable trend. However, across all runs the maximum error was 10.6% at a COM error of 19.1%, which is similar to the error observed in the other MOIs at much lower COM errors. In general, I_{yy} and I_{zz} both show greater sensitivity than I_{xx} as the errors seen in the latter two are noticeably higher once 5% location error is reached. Taken together, these results highlight the need of accurate known quantities to calculate accurate MOIs, although the lack of a clear trend in the I_{xx} data shows that the exact relation may be dependent on other factors as well.

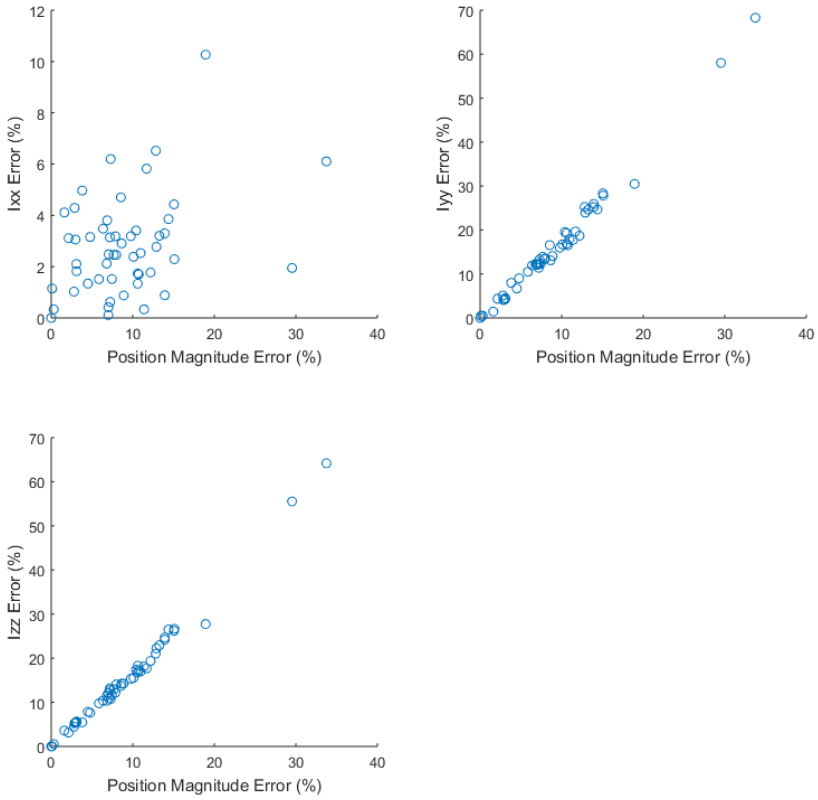

Figure 8: MOI Absolute Error for Varying COM Locations (Dumbbell)

Varying System Mass

For these cases, the mass of the combined system was varied from the true value of 25000 kg to investigate its effect on the MOI calculations. The percent error in each MOI is plotted against the total system mass error, which is a percentage calculated by finding the absolute difference in the total system mass for the given case and the true mass, then normalizing it with respect to the true mass. For all three principal MOIs, up to about a 5% error in mass, the error increases relatively linearly at approximately the same rate. However, soon after that the I_{yy} and I_{zz} split into two curves that slowly diverge from each other as the mass error increases, as seen in Fig. 9. I_{xx} does not share this behavior and continues to increase at roughly the same rate as at the lower

mass errors. The splitting is a result of taking the absolute value of the MOI error and the positive and negative errors propagating at slightly different rates as a function of the system mass error. Regardless of the split, these results are similar to the COM errors in that limiting the mass error to 10% limits the MOI errors to 10%-15% while higher mass errors quickly lead to more drastic MOI errors.

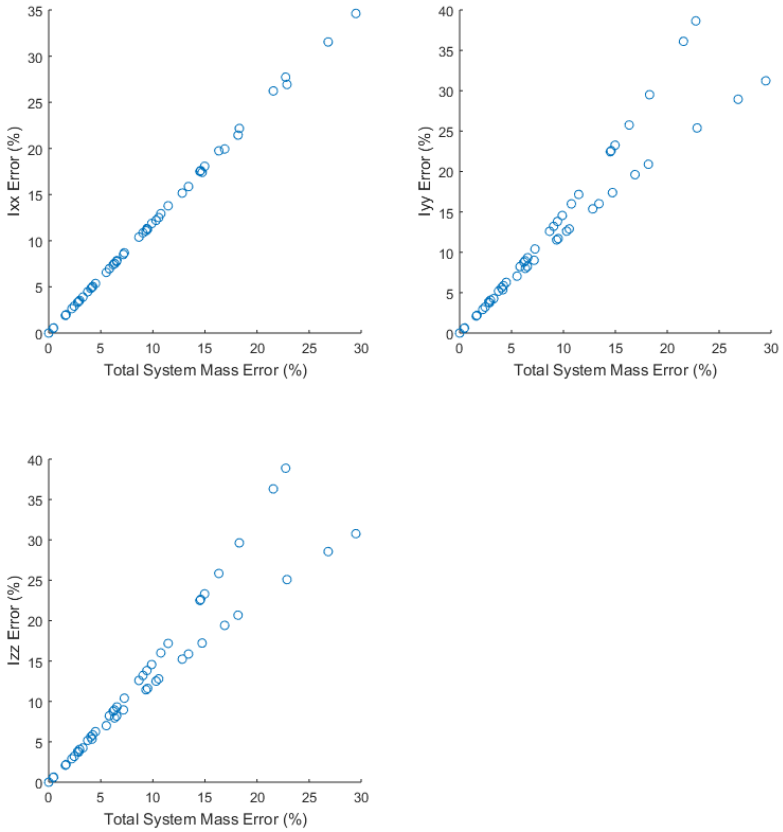

Figure 9: MOI Absolute Error for Varying Total System Mass (Dumbbell)

Spherical Model

For this series of results the dumbbell asteroid model previously used has been replaced with the spherical asteroid model. Although spherical asteroids tend to be larger enough to be considered dwarf planets in some cases, this model will have a radius of 1.5m and a mass of 10000kg. This is done to keep the size comparable to the dumbbell asteroid model discussed prior and make any variations in the results due to the change in geometry and not mass. The same cylindrical spacecraft model is used here as well.

Varying Center-of-Mass Location

The MOI error from varying the COM location for the spherical asteroid system demonstrates slightly different behavior than the dumbbell model due to the sphere's symmetry about all three axes. The I_{yy} and I_{zz} errors see a similar linear growth to the dumbbell model, while the I_{xx} has virtually zero error across all 50 cases as seen in Fig. 10. This is most likely a result of the complete symmetry of the sphere, which allows its principal axes to be defined in infinite orientations, so there can always be one axis in complete alignment with one of the spacecraft. At 10% position magnitude error, the I_{yy} and I_{zz} errors are near 15% once again, showing a consistency in the calculation's sensitivity to errors in the known mass properties, partially independent of model geometry.

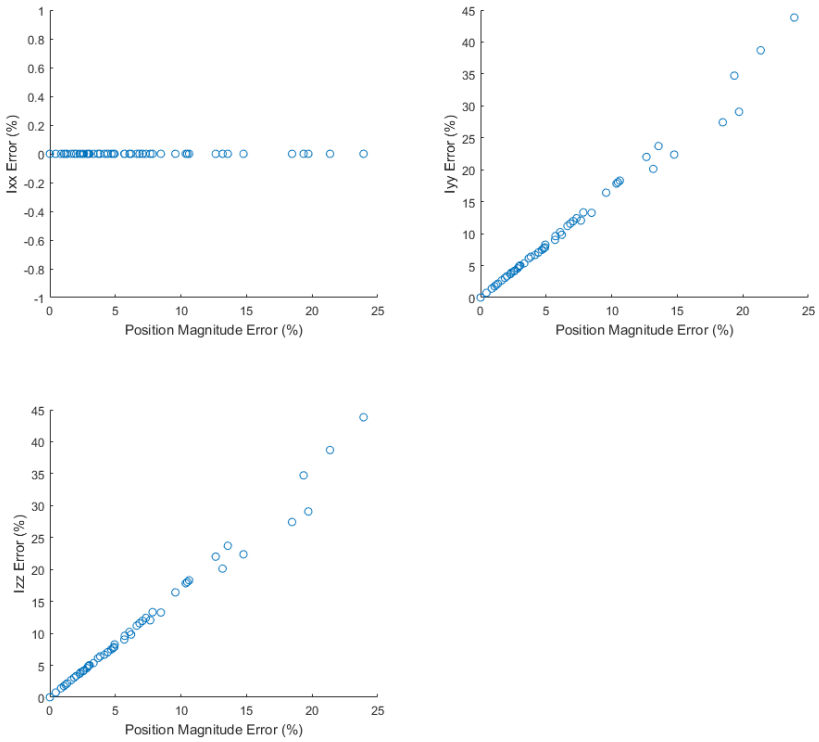

Figure 10: MOI Absolute Error for Varying COM Locations (Spherical)

Varying System Mass

Varying the total system mass yields similar results to the dumbbell model in Figure 11, despite the very different geometry of the asteroids. A 10% uncertainty in the system mass causes a 10-15% error across the $\boldsymbol{I_{yy}}$ and $\boldsymbol{I_{zz}}$, while $\boldsymbol{I_{xx}}$ error is again closer to 8%. The split in $\boldsymbol{I_{yy}}$ and $\boldsymbol{I_{zz}}$ the curves due to taking the absolute error is present as well, although the lack of data points past 15% mass error prevent any founded conclusions on the similarity between the two models to be made in that region.

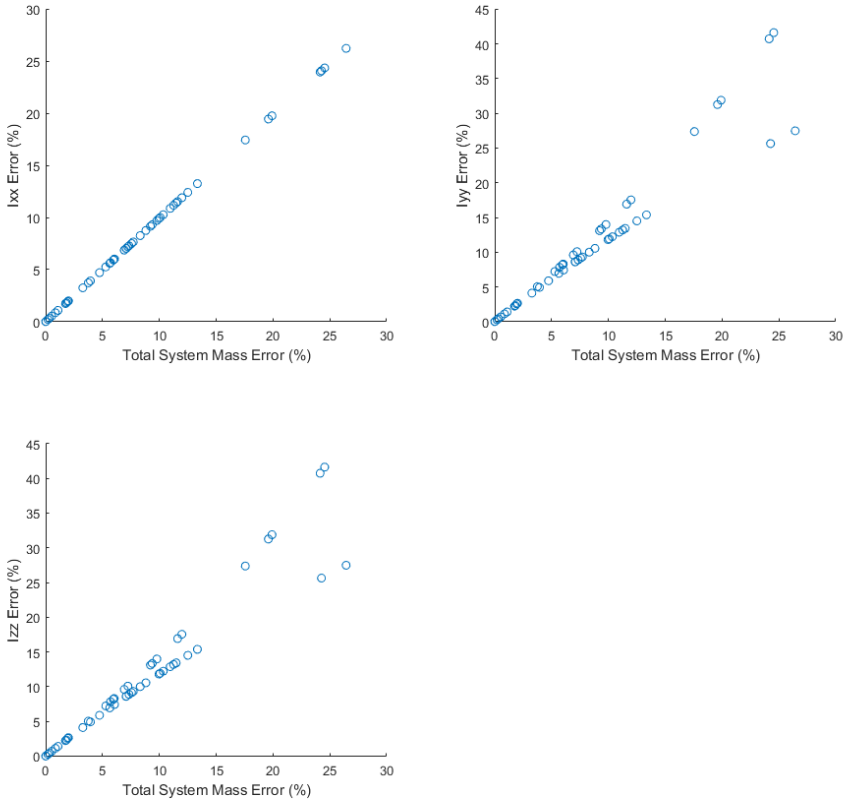

Figure 11: MOI Absolute Error for Varying Total System Mass (Spherical)

Average Errors for all Variation Options

Looking at the MOI error for each component averaged across all 50 cases supports many of the conclusions drawn from the graphs presented earlier. The $\boldsymbol{I_{yy}}$ and $\boldsymbol{I_{zz}}$ errors for the dumbbell model and all types of variations remain very similar, while they are identical for the spherical model due to its symmetry about all axes. Uncertainty in the system mass have a much greater impact on the MOI along the x-axis than the COM location error, while the other MOIs are only

slightly more sensitive to COM variations. Varying both quantities actually reduced the average error for $\boldsymbol{I_{xx}}$, but increased the error in the other two MOIs by roughly 8%-9%.

Table 3: Average MOI Errors

Varying Center-of-Mass Location			
Model	$\boldsymbol{I_{xx}}$	$\boldsymbol{I_{yy}}$	$\boldsymbol{I_{zz}}$
Dumbbell	2.46%	11.86%	11.14%
Spherical	0.00%	12.01%	12.01%
Varying System Mass			
Model	I_{xx}	I_{yy}	I_{zz}
Dumbbell	9.45%	10.82%	10.80%
Spherical	8.11%	10.59%	10.59%
Varying Both			
Model	I_{xx}	I_{yy}	I_{zz}
Dumbbell	8.21%	19.27%	19.58%
Spherical	7.39%	18.37%	18.37%

Chapter 7

Conclusions and Future Work

The goal of this thesis was to determine the principal MOIs and principal axes of a combined spacecraft-asteroid system utilizing previously known mass properties. These new mass properties need to be known with relative accuracy to serve as an initial estimation that can be used to develop a control scheme for the combined system in the future. Based on these results from the dumbbell asteroid model, larger errors in both COM location and system mass do result in greater MOI errors, making it critical to have as accurate of measurements as possible. Both COM location and system mass should be known to within 10% or less in order to keep all three principal MOIs to within 15% of their true values. Utilizing a spherical model for the asteroid of the same mass, shows similar sensitivity in the principal MOIs, suggesting that this calculation method is fairly insensitive to the model geometry.

Work in the near future will investigate asteroids of larger size and higher density to see if this technique has any size limitations. It will also look at how other, less symmetric geometric models for the asteroid and spacecraft may impact the reliability of this method. While the principal axes are simply the eigenvectors found from the associated eigenvalues (principal MOIs), directly calculating the errors between them proved outside the scope of this thesis, making this another extension needed for fully investigate the accuracy of this method.

Long term future work is needed to develop a process to refine the inertia tensors of the asteroid and combined system based on this initial estimate. One potential technique would be to utilize small, controlled thrusts along each spacecraft axis to change the rotational speed of the system. By knowing the spacecraft's relative location with respect to the system's center-of-mass, the thrust applied, and the initial estimation of the inertia tensor, the expected angular acceleration

can be calculated. Accelerometers on the spacecraft can be used to detect the actual angular acceleration of the system. Any discrepancies in acceleration must then be the result of an incorrect inertia tensor. Using iterative methods, the inertia tensor values could then be adjusted until the predicted acceleration agrees with the actual accelerometer values.

REFERENCES

[1] Beshore, E., Lauretta, D., Boynton, W., Shinohara, C., Sutter, B., Everett, D., Gal-Edd, J. S., Mink, R. G., Moreau, M., and Dworkin, J., "The OSIRIS-REx Asteroid Sample Return Mission," IEEE 2015 Aerospace Conference, Mar. 2015.

[2] "Luxembourg eyes asteroid mining," *Science*, vol. 354, Nov. 2016, pp. 686–687.

[3] Misiak, M., "Cosmic Engineering: Moving Asteroids," International Journal of Astronomy and Astrophysics, vol. 03, 2013, pp. 517–519.

[4] Wittick, P., "Attitude Dynamics Modeling for Docking Operations with Uncooperative Objects", B.S. Thesis, Department of Aerospace Engineering, The Pennsylvania State University, May 2015.

[5] Liang, J., and Ma, O., "Angular velocity tracking for satellite rendezvous and docking," Acta Astronautica, vol. 69, 2011, pp. 1019–1028.

[6] Ďurech, J., Sidorin, V., and Kaasalainen, M., "DAMIT: a database of asteroid models," Astronomy and Astrophysics, vol. 513, 2010.

[7] Thomas, P. C., Binzel, R. P., Gaffey, M. J., Zellner, B. H., Storrs, A. D., and Wells, E., "Vesta: Spin Pole, Size, and Shape from HST Images," Icarus, vol. 128, 1997, pp. 88–94.

[8] Mission Evaluation Team, "Apollo 13 Mission Report," NASA MSC-02680, September 1970.

[9] Curtis, H. D., Orbital mechanics for engineering students, Amsterdam: Elsevier, 2014.

ACADEMIC VITA

Robert Vitagliano

1208 Ash Court
Hazle Township, PA 18202

570-579-3026
robv2525s@gmail.com

EDUCATION

The Pennsylvania State University, Schreyer Honors College, University Park, PA
Bachelor of Science, Aerospace Engineering
Graduation: Spring 2018

PROFESSIONAL EXPERIENCE

Engineering Intern — May – Aug. 2017
Wyman Gordon, Mountain Top, PA

- Responsibilities included designing and drafting parts used in industrial welding equipment, obtaining quotes for part fabrications, and optimizing work flow
- Organized tooling storage facilities for two company locations and created basic Access database to digitize storage record system

RESEARCH PROJECTS

Schreyer Honors College Senior Thesis, — Aug. 2017-Present
Penn State University Park

- Researching how to determine mass properties of uncooperative asteroids using sensors from a docked spacecraft
- Developing models for the asteroid/spacecraft, testing the solution algorithm, and performing error analysis

MC REU Program, Penn State Hazleton — May 2016-Aug. 2016

- Researched the validity of smartphone based solar surveying applications and performed a comparative analysis of said applications against commercial tools
- Presented findings at a research symposium, constructed a professional poster, and wrote a brief thesis

Solar Research Project (ENGR 296H), Penn State Hazleton — Aug. 2015–Sept.2016

- Wrote code to simulate objects on the horizon that would interfere with the collection of sunlight
- Performed numerical data analysis to determine the effect surveying errors will cause in the calculations

AFFILIATIONS

Tau Beta Pi (PA Beta Chapter) – Vice President	Spring 2017-Present
Innovative Design Club – Vice President	Fall 2016 – Present
Sigma Gamma Tau (Aerospace Honors Society) – Member	Spring 2017-Present
Student Government Association – President	Fall 2014-Spring 2016

HONORS & AWARDS

1st Place Penn State Hazleton Research Fair	Spring 2016
Penn State University President's Sparks Award	Spring 2016
PSU Hazleton Student Government Assoc. Appreciation Award	2015-2016
Penn State University Academic Achievement Award	Spring 2015

PUBLICATIONS

Joseph Ranalli, Robert Vitagliano, Mauro Notaro, David J. Starling, Sensitivity of shading calculations to horizon uncertainty, Solar Energy, Volume 144, 1 March 2017, Pages 399-410, ISSN 0038-092X, http://dx.doi.org/10.1016/j.solener.2017.01.017.